Journal of the Korean Physical Society, Vol. 57, No. 6, December 2010, pp. 1942∼1945

Simulation Study of Sub-10 nm Pattern Formation Using Diblock Polymer Directed Self-assembly

Sang-Kon Kim,* Hye-Keun Oh, Young-Dae Jung and Ilsin An
Department of Applied Physics, Hanyang University, Ansan 426-791

(Received 15 January 2010, in final form 30 October 2010)

Because top-down approaches, such as the extreme ultraviolet technique and high-index fluid-based immersion ArF lithography, may cover one or two generations, lithography technology for scaling down feature size to sub-10-*nm* is becoming more complex. The directed self-assembly technology of block copolymers is one candidate for next-generation lithography. In this paper, a directed self-assembly lithography process for block copolymers is modeled and simulated on a molecular scale to solve the challenges associated with directed self-assembly technology. Sub-10-*nm* patterns can be formed by using precise pattern placement of a conventional 'top-down' optical lithography with the well-defined nanostructure and self-healing properties of 'bottom-up' block copolymer self-assembly. Simulation results matched the experiment results.

PACS numbers: 85.40.Hp, 78.20.Bh, 07.10.Cm, 81.16.Nd, 07.05.Tp
Keywords: Lithography, Lithography simulation, Self-assembly, Self-assembly process, Block copolymer
DOI: 10.3938/jkps.57.1942

I. INTRODUCTION

For 32-*nm* and 22-*nm* pattern formation, top-down approaches are extreme ultraviolet lithography (EUVL), high-index fluid-based immersion ArF lithography, and double patterning technology (DPT). According to the ITRS (international technology roadmap for semiconductors), the challenges of 22-*nm* pattern formation are topcoat development, resist refractive >1.8, and fluid refractive >1.65 for immersion lithography. For EUVL, the challenges are low defect mask, source power >180 W, and linewidth roughness (LWR) <3 *nm*. For DPT, the challenges are overlay of multiple exposures, availability of software to split the pattern, and a photoresist with independent exposure. For below 10-*nm* pattern formation, those top-down approaches are limited, and a bottom-up technology is required. A promising technique to achieve this scaling is block copolymer (BCP) lithography, which affords 10-*nm* to 30-*nm* feature sizes [1].

BCP thin films with spherical, cylindrical, or lamellar morphologies of different length scales may be created by adjusting the composition and molecular weight of the BCP [2, 3]. Block copolymers have been suggested for many applications based principally on their ability to form regular nanometer-scale patterns. These self-assembled patterns have been considered for nanolithographic masks, as well as templates, for further preparation of inorganic or organic structures [4]. BCP lithography is attractive because it can be done under simplified processing conditions with no requirement for expensive projection tools. The challenge of BCP lithography, however, is low critical dimension variation, low edge roughness, high throughput, low number density of pattern defects, scale down to sub-10-*nm* domain sizes, long-range order formation of regular patterns, and control of multi-level (three-dimension) assembly. Mesoscale simulations and molecular simulations can be useful for predicting self-assembled structures in various macromolecular systems and for ordering of molten block copolymer. To now, there are no papers on full simulations of BCP lithography. In this research, a simulation of optical lithography for template fabrication and a mesoscale simulation for BCP lithography with this template were performed.

II. MODELING OF BLOCK COPOLYMER LITHOGRAPHY

Block copolymers, such as diblock (A-block-B), triblock (A-block-B-block-A), and multi-block (-(A-B)n-), covalently link two or more polymer chains. Block copolymers produce lamellar, cylindrical, spherical, and gyroid microdomains due to the thermodynamic incompatibility and connectivity of the block components [2, 3]. The phase behavior and final morphology of block copolymers is determined by the volume fraction of one

*Email: sangkona@hotmail.com, http://www.sangkon.info

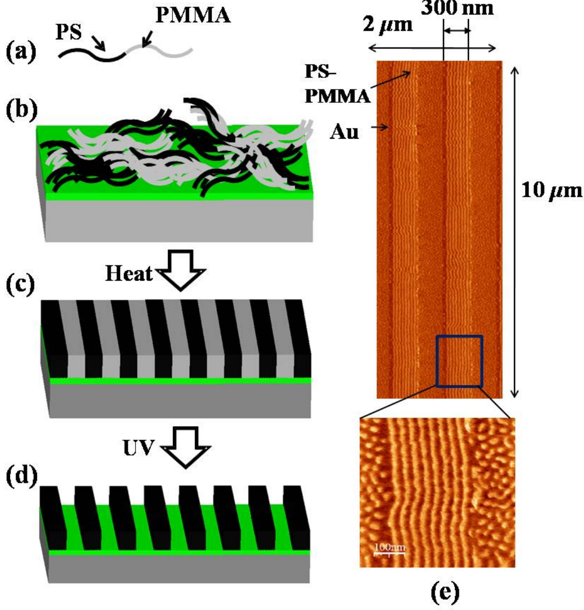

Fig. 1. (Color online) Pattern formation flow of self-assembly block copolymers: (a) polystyrene-*block*-poly (methyl methacrylate) copolymers (PS-*b*-PMMA), (b) spin-coating of PS-*b*-PMMA, (c) linear alignment of PS-*b*-PMMA by annealing, (d) selective removal of PMMA blocks with acetic acid by irradiation with an ultraviolet source, and (e) experimental results of Ref. 5 for patterning block copolymers.

block (f), the Flory-Huggins interaction parameter (χ) between the blocks, the total number of segments (or the degree of polymerization) (N), and the surface tensions and the interfacial tensions of both blocks with the substrate.

Figure 1 shows the pattern formation flow for block copolymers. The block copolymer in Fig. 1(a) is a polystyrene-*block*-poly (methyl methacrylate) copolymer (PS-*b*-PMMA). After spin-coating of PS-*b*-PMMA in Fig. 1(b), PS-*b*-PMMA in Fig. 1(c) is annealed for linear formation. The linear PMMA blocks with acetic acid in Fig. 1(d) are removed by irradiation with an ultraviolet source and lithography processes. Figure 1(e) shows the experimental results for block copolymers deposited on nano-patterned substrates in Ref. 5. Au patterns with 300-nm trenches were prepared by using DUV lithography, Au deposition, and Au lift-off. The block copolymers were deposited on these nano-patterned substrates. The properties of the P(S-*b*-MMA) molecular structure are Mn PS (43,500 g/mol), Mn PMMA (21,000 g/mol), Mw/Mn=1.09, Tg of PS = 105 °C, and Tg of PMMA = 115 °C (polymer source) [5].

Figure 2 shows the process simulation for template fabrication by using optical lithography. The simulation results are 75-nm and 10-μm line and space (L/S) pattern formations in a positive chemical amplified resist (CAR). The internal results are the intensity distribution in Fig. 2(a) [6], the photoacid generator (PAG) concentrations after exposure process in Fig. 2(b), the cross-linked concentrations after post exposure bake (PEB) in Fig. 2(c), the dissolution rate concentrations after development in Fig. 2(d), and the pattern profiles in Fig. 2(f) [7,8]. Simulation results are in good agreements with experimental results. For a 75-nm (L/S = 1:1) pattern formation, experimental conditions corresponding to the simulation conditions are a 193-nm wavelength, a 240-nm resist thickness, 0.7 NA, dipole illumination with 0.567 σ_{in}, 0.85 σ_{out}, and 90 degrees, and a 0.1-μm (L/S = 1:1) 6% Att-PSM mask [9]. For the 10-μm (L/S = 1:1) pattern formation, experiment conditions corresponding to simulation conditions are a 365-nm wavelength, 0.48 NA, a 40-μm resist thickness, soft bake (SB) at 110 °C for 300 sec, PEB at 90 °C for 120 sec, and development for 60 sec [10].

Figure 3 shows a potential interaction of particles due to time. For a molecular dynamics method, the equations of motion (Newtons equations) are solved for atoms as

$$m_i \frac{d^2\vec{r}_i}{dt^2} = \vec{F}_i = -\nabla_i \phi(r) = 4\varepsilon \left[\left(\frac{\sigma}{r}\right)^{12} - \left(\frac{\sigma}{r}\right)^{6} \right], \quad (1)$$

where m_i is the mass, r_i is the position vector, F_i is the force vector of a molecule i, $\phi(r)$ is the Lennard-Jones potential function as the system potential, ε is the energy, σ is the length scale, and r is the intermolecular distance. Ar particles are more active than Ne particles because the length scale of Ar is larger than that of Ne in Fig. 3.

Figure 4 shows the lamellar phase behavior of a block copolymer due to the dimensionless parameters ($1/T^*$): 0.1, 0.024, 0.016, and 0.01. T^* is the temperature, the number of block copolymers is 125, and the simulation volume is 18.26 × 18.26 × 18.26 when the block copolymer size is one unit. In Fig. 4, a simple model can describe the formation of a lamellar morphology due to temperature.

III. COMPARISON OF SIMULATION RESULTS WITH EXPERIMENT RESULTS

According to a mean-field approximation for the equilibrium density distributions [11], the modified diffusion equations for the propagators are

$$\left[-\varepsilon_A \beta \nabla^2 + \omega_A'(\vec{r})\right] Q_A\left(\vec{r}, \tau | \vec{r}'\right) = -\frac{1}{f_A}\frac{\partial}{\partial \tau} Q_A\left(\vec{r}, \tau | \vec{r}'\right), \quad (2)$$

$$\left[-\varepsilon_B \beta \nabla^2 + \omega_B'(\vec{r})\right] Q_B\left(\vec{r}, \tau | \vec{r}'\right) = -\frac{1}{f_B}\frac{\partial}{\partial \tau} Q_B\left(\vec{r}, \tau | \vec{r}'\right), \quad (3)$$

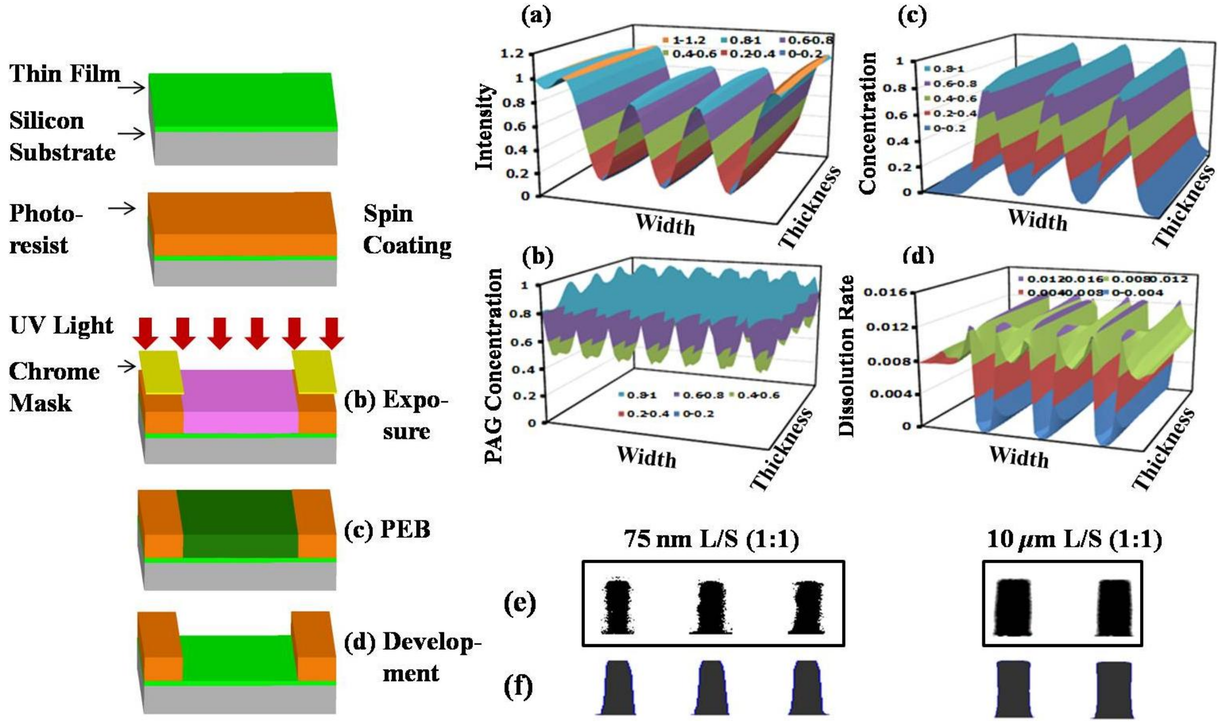

Fig. 2. (Color online) Process simulation of the template fabrication for the micro-/-nano L/S pattern formation: For a positive resist, (a) intensity distribution in the top resist, (b) PAG concentrations after the exposure process, (c) cross-linked concentrations after the PEB process, (d) development rate concentrations after the develop process, (e) experimental results [9,10], and (f) simulation results for a 75-nm 1:1 L/S pattern and 10-μm 1:1 L/S pattern.

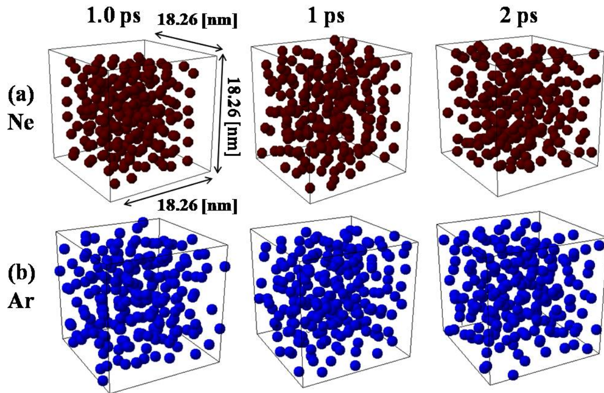

Fig. 3. (Color online) Potential interactions of Ne and Ar particles at 0.1 ps, 1 ps, and 2 ps: (a) for 216 particles of Ne, $\sigma = 0.274$ nm, $\varepsilon = 0.50\times10^{-21} J$, and $\varepsilon k_B = 36.5$ K; (b) for 216 particles of Ar, $\sigma = 0.34$ nm, $\varepsilon = 1.67\times10^{-21} J$, and $\varepsilon k_B = 121$ K.

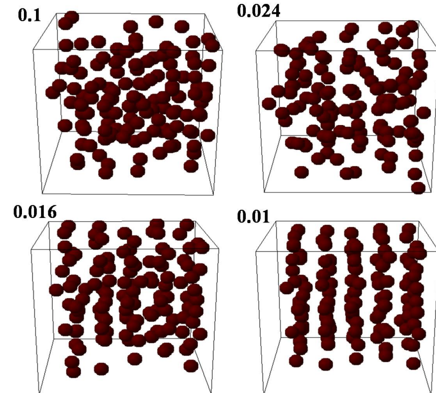

Fig. 4. (Color online) Snapshots of lamellar morphology formation due to dimensionless parameters ($1/T^*$): 0.1, 0.024, 0.016, and 0.01. T^* is the dimensionless temperature.

where $\beta = r_c\rho_{0A}b_A^2/6\rho_0 R^2$, R is a given lattice constant, r_0 is the reference density used in defining the Flory parameter χ, ρ_{0A}, and ρ_{0B} are pure component densities, b_A and b_B are Kuhn statistical lengths, the effective degree of polymerization is $r_C = r_A + r_B$, which consist of $r_A = \rho_0 N_A/\rho_{0A}$ and $r_B = \rho_0 N_B/\rho_{0B}$, the block degrees of polymerizations are $N_B = N - N_A$, $\varepsilon_A = 1$, $\varepsilon_B \equiv \varepsilon = \rho_{0B}b_B^2/\rho_{0A}b_A^2$, the fraction of A segments per chain is $f_A{=}r_A/r_C \equiv \bar{\phi}_A$, and the fraction of B segments per chain is $f_B = r_B/r_C \equiv \bar{\phi}_B$. The periodic boundary conditions are

$$Q_p\left(\vec{r}, 0|\vec{r}'\right) = \sum_n \delta\left(\vec{r} - \vec{r}' - \vec{R}_n\right), \tag{4}$$

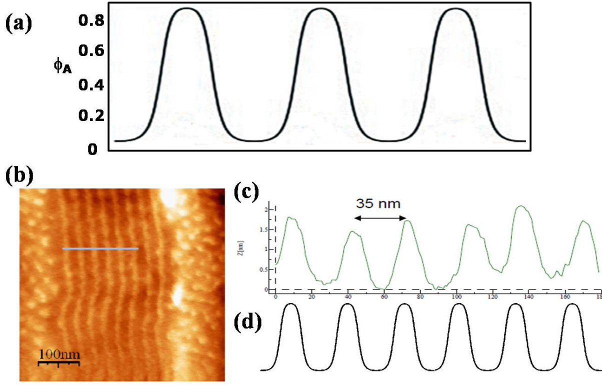

Fig. 5. (Color online) Comparison of simulation results with experiment results: (a) the dimensionless concentration of the diblock system of A segment ϕ_A, (b) and (c) experiment results [5], and (d) simulation result for the dimensionless concentration profile.

where R_n is a set of lattice vectors. The potentials are

$$\begin{aligned} \omega_A^{'}(\vec{r}) &= \chi r_C \left[\phi_B(\vec{r}) - \vec{\phi}_B\right] + \eta^{'}(\vec{r}), \\ \omega_B^{'}(\vec{r}) &= \chi r_C \left[\phi_A(\vec{r}) - \vec{\phi}_A\right] + \eta^{'}(\vec{r}), \end{aligned} \tag{5}$$

where the Lagrange multiplier field associated with the incompressibility is

$$\eta^{'}(\vec{r}) = \rho_0^2 \left(\frac{\omega_A^{'}(\vec{r}) + \omega_A^{'}(\vec{r})}{2} \right). \tag{6}$$

The dimensionless concentration profile of a diblock system of A is

$$\phi_A(\vec{r}) = \frac{\bar{\phi}_A V}{Q_C^{'}} \int_0^1 d\tau q_A(r,\tau)\, \tilde{q}_B(r, 1-\tau), \tag{7}$$

where $\phi_A(\vec{r}) + \phi_B(\vec{r}) = 1$, $\tilde{q}_B(r, 1-\tau) = \int d\vec{r}^{'} Q_A \left(\vec{r}, 1-\tau|\vec{r}^{'}\right) q_B\left(\vec{r}^{'}, 1\right)$, $q_p(\vec{r},\tau) = \int_\Omega d\vec{r}^{'} Q_p\left(\vec{r},\tau|\vec{r}^{'}\right)$, $Q_C^{'} \,/\, V = \int_1^0 dr q_A(r,1)\, q_B(r,1)$, and V is the volume of the system.

Figure 5 shows a comparison of the simulation results with the experiment results. Figure 5(a) shows the concentration ϕ_A of the A segment in the diblock system. Simulation results with $f = f_A = f_B = 0.5$ and $\chi N = 20$ can be matched to the simulation results.

IV. CONCLUSION

For nano-pattern formation, the pattern formation of self-assembly block copolymers is modeled and simulated by using a molecular-scale modeling method. Simulation results can be matched to experiment results. The simulation can be used to optimize the process conditions for self-assembly block copolymers and to develop the self-assembly technology.

ACKNOWLEDGMENTS

This research was supported by Basic Science Research Program through the National Research Foundation on Korea (NRF) funded by the Ministry of Education, Science and Technology (2009-0074676).

REFERENCES

[1] C. Tang, E. M. Lennon, G. H. Fredrickson, E. J. Kramer and C. J. Hawker, Science **322**, 429 (2008).
[2] C. Park, J. Yoon and E. L. Tomas, Polymer **44**, 6725 (2003).
[3] R. A. Segalman, Mater. Sci. Eng., R **48**, 191 (2005).
[4] T. Thurn-Albrecht, J. Schotter, G. A. Kastle, N. Emley, T. Shibauchi, L. Krusin-Elbaum, K. Guarini, C. T. Black, M. T. Tuominen and T. P. Russell, Science **290**, 2126 (2000).
[5] I. Dika, A. Dirani and O. Soppera, in *Proceedings of the 35th International Conference on Micro nano Engineering (MNE)* (Belgium, Sepember 28, 2009), P-LITH-48.
[6] S.-K. Kim, J. Korean Phys. Soc. **50**, 1952 (2007).
[7] S.-K. Kim and H.-K. Oh, J. Korean Phys. Soc. **41**, 456 (2002).
[8] S.-K. Kim, H.-K. Oh, Y.-D. Jung and I. An, J. Korean Phys. Soc. **55**, 2, 661 (2009).
[9] G. Capetti, M. Bollin, A. Pepe, G. Cotti, S. Loi and U. Iessi, Proc. SPIE **5377**, 881 (2004).
[10] M. Toukhy, M. Paunescu, Z. Bogusz and G. Pawlowski, Proc. SPIE **7273**, 72730J-1 (2009).
[11] R. B. Thompson, V. V. Ginzburg, M. W. Matsen and A. C. Balazs, Macromolecules **35**, 1060 (2002).